Contents lists available at ScienceDirect

Solid State Communications

The Kohn–Luttinger superconductivity in idealized doped graphene

M.Yu. Kagan [a,b], V.V. Val'kov [c], V.A. Mitskan [c,d], M.M. Korovushkin [c]

[a] P.L. Kapitza Institute for Physical Problems, 119334 Moscow, Russia
[b] Moscow Institute of Electronics and Mathematics, National Research University Higher School of Economics, 109028 Moscow, Russia
[c] L.V. Kirensky Institute of Physics, 660036 Krasnoyarsk, Russia
[d] Siberian State Aerospace University, 660014 Krasnoyarsk, Russia

ABSTRACT

Idealized graphene monolayer is considered neglecting the van der Waals potential of the substrate and the role of the nonmagnetic impurities. The effect of the long-range Coulomb repulsion in an ensemble of Dirac fermions on the formation of the superconducting pairing in a monolayer is studied in the framework of the Kohn–Luttinger mechanism. The electronic structure of graphene is described in the strong coupling Wannier representation on the hexagonal lattice. We use the Shubin–Vonsowsky model which takes into account the intra- and intersite Coulomb repulsions of electrons. The Cooper instability is established by solving the Bethe–Salpeter integral equation, in which the role of the effective interaction is played by the renormalized scattering amplitude. The renormalized amplitude contains the Kohn–Luttinger polarization contributions up to and including the second-order terms in the Coulomb repulsion. We construct the superconductive phase diagram for the idealized graphene monolayer and show that the Kohn–Luttinger renormalizations and the intersite Coulomb repulsion significantly affect the interplay between the superconducting phases with f-, $d+id$-, and $p+ip$-wave symmetries of the order parameter.

© 2014 Elsevier Ltd. All rights reserved.

1. Introduction

One of the most interesting properties of graphene is controllability of the position of its chemical potential by an applied electric field, which allows the change of the carrier type (electrons or holes) [1,2]. It was experimentally demonstrated that short graphene samples placed between superconducting contacts could be used for constructing Josephson junctions [3]. This indicates that Cooper pairs can coherently propagate in graphene. The question now arises of whether graphene can be structurally or chemically modified to become a magnet [4] or even a true superconductor.

Theoretically, a model with the conical dispersion requires the minimum intensity of the pairing interaction to develop the Cooper instability [5]. In view of this fact, a number of attempts were made to theoretically analyze possible implementation of the superconducting state in doped graphene. In paper [6], the role of topological effects in implementation of the Cooper pairing in this material was investigated. In paper [7], using the mean field approximation, the plasmon type of superconductivity in graphene was investigated, which leads to the low critical temperatures in the s-wave channel for realistic electron densities. The

possibility of inducing superconductivity in graphene by electron correlations was studied in [8,9]. In paper [10], the interplay of the superconducting phase with the $d+id$-wave symmetry of the order parameter and the spin density wave phase depending on the position of the chemical potential with respect to van Hove singularity in the electron density of states of graphene was investigated using the functional renormalization group. Near the van Hove singularity, the superconducting phases with $d+id$- and f-wave symmetries of the order parameter were found.

In paper [11], the situation was considered when the Fermi level is located near one of the van Hove singularities in the density of states of graphene. It is known that these singularities can enhance the magnetic and superconducting fluctuations [12]. According to the scenario described in [11], the Cooper instability occurs due to the strong anisotropy of the Fermi contour at van Hove filling n_{vH}, which, as a matter of fact, originates from the Kohn–Luttinger mechanism [13] proposed in 1965 suggesting the appearance of the superconducting pairing in systems with the purely repulsive interaction. According to the estimation made in [11], the Cooper instability of this type in idealized graphene can increase the critical temperatures of the superconducting transition up to 10 K, depending on whether the chemical potential level is close to the van Hove singularity. It should be noted that in the calculation only the Coulomb repulsion of electrons on one site was taken into account. In paper [14], the possible interplay and coexistence of the Pomeranchuk instability and the

E-mail addresses: kagan@kapitza.ras.ru (M.Yu. Kagan),
vvv@iph.krasn.ru (V.V. Val'kov).

Kohn–Luttinger superconducting pairing in graphene were discussed. The authors of [15] demonstrated using a renormalization group approach within the Kohn–Luttinger mechanism that in a monolayer of the doped graphene the superconducting $d+id$-pairing can be implemented.

In this paper, an idealized monolayer of graphene is considered neglecting the van der Waals potential of the substrate and the role of the nonmagnetic impurities. The Cooper instability in a monolayer is investigated in the weak coupling limit of the Born approximation by implementing the Kohn–Luttinger mechanism with respect to the Coulomb repulsion of electrons localized not only on one, but also on the nearest-neighbor carbon atoms. In the evaluation of the effective interaction in the Cooper channel, we take into account the polarization contributions caused by the Coulomb repulsion between electrons belonging to both one and different branches of the graphene energy spectrum.

The necessity to account for the long-range Coulomb repulsion in the calculation of the physical characteristics of graphene was dictated by the results of paper [16], where in the ab initio calculation of the effective many-body model of graphene and graphite the values of the partially screened frequency-dependent Coulomb repulsion were determined. It was demonstrated that the value of the onsite repulsion in graphene is $U=9.3$ eV and the Coulomb repulsion of electrons localized on the neighboring sites is $V=5.5$ eV, which indicates the principle importance to take into account the nonlocal Coulomb interaction. Note that other researchers consider the values of U and V to be much smaller.

2. Theoretical model

Since there are two carbon atoms per each unit cell of the graphene lattice, the latter can be divided in two sublattices A and B. In the Wannier representation, the Hamiltonian of the Shubin–Vonsowsky model (the extended Hubbard model) [17] for graphene with respect to electron hoppings between the nearest-neighbor and next-to-nearest-neighbor atoms and the Coulomb repulsion of electrons located at one and at neighboring sites has the form

$$\hat{H} = \hat{H}_0 + \hat{H}_{int}, \tag{1}$$

$$\hat{H}_0 = -\mu \sum_f (\hat{n}_f^A + \hat{n}_f^B) - t_1 \sum_{\langle fm \rangle \sigma} (a_{f\sigma}^\dagger b_{m\sigma} + \text{h.c.})$$
$$- t_2 \sum_{\langle\langle fm \rangle\rangle \sigma} (a_{f\sigma}^\dagger a_{m\sigma} + b_{f,\sigma}^\dagger b_{m,\sigma} + \text{h.c.}), \tag{2}$$

$$\hat{H}_{int} = U \sum_f (\hat{n}_{f\uparrow}^A \hat{n}_{f\downarrow}^A + \hat{n}_{f\uparrow}^B \hat{n}_{f\downarrow}^B) + V \sum_{\langle fm \rangle} \hat{n}_f^A \hat{n}_m^B. \tag{3}$$

Here $a_{f\sigma}^\dagger(a_{f\sigma})$ are the operators that create (annihilate) an electron with the spin projection $\sigma = \pm 1/2$ at site f of the sublattice A, $\hat{n}_f^A = \sum_\sigma \hat{n}_{f\sigma}^A = \sum_\sigma a_{f\sigma}^\dagger a_{f\sigma}$ are the operators of the numbers of fermions at site f of the sublattice A (the analogous notations are used for the sublattice B), μ is the chemical potential of the system, t_1 is the hopping integral between neighboring atoms (hoppings between different sublattices), t_2 is the hopping integral between the next-to-nearest-neighbor atoms (within one sublattice), U is the parameter of the Coulomb repulsion of electrons located at one site and having the opposite spin projections (Hubbard repulsion), and V is the Coulomb repulsion of electrons located at neighboring atoms. In the Hamiltonian, $\langle \rangle$ denotes the summation over the nearest neighbors only, $\langle\langle \rangle\rangle$ denotes the summation over the next to nearest neighbors.

After the transition to the momentum state and the Bogoliubov transformation

$$\alpha_{i,k,\sigma} = w_{i1}(k) a_{k,\sigma} + w_{i2}(k) b_{k,\sigma}, \quad i = 1, 2, \tag{4}$$

the Hamiltonian $\hat{H}_0$ is diagonalized and acquires the form

$$\hat{H}_0 = \sum_{i=1}^{2} \sum_{k\sigma} E_{i,k} \alpha_{i,k,\sigma}^\dagger \alpha_{i,k,\sigma}. \tag{5}$$

The two-band energy spectrum of graphene is described by the expressions [18]

$$E_{1,k} = t_1 |u_k| - t_2 f_k, \quad E_{2,k} = -t_1 |u_k| - t_2 f_k, \tag{6}$$

where the notations

$$f_k = 2 \cos(\sqrt{3}k_y) + 4 \cos\left(\frac{\sqrt{3}}{2}k_y\right) \cos\left(\frac{3}{2}k_x\right),$$

$$u_k = \sum_\delta e^{ik\delta} = e^{-ik_x} + 2e^{(i/2)k_x} \cos\left(\frac{\sqrt{3}}{2}k_y\right), \quad |u_k| = \sqrt{3 + f_k} \tag{7}$$

were used. The Bogoliubov transformation parameters have the form:

$$w_{1,1}(k) = w_{22}^*(k) = \frac{1}{\sqrt{2}} r_k^*, \quad r_k = \frac{u_k}{|u_k|},$$

$$w_{12}(k) = -w_{21}(k) = -\frac{1}{\sqrt{2}}. \tag{8}$$

In the Bogoliubov representation of quasiparticles, the interaction operator (3) is determined by the expression containing $\alpha_{1,k,\sigma}$ and $\alpha_{2,k,\sigma}$ as

$$\hat{H}_{int} = \frac{1}{N} \sum_{\substack{i,j,l,m \\ k,p,q,s,\sigma}} \Gamma_{ij;lm}^\parallel(kp|qs) \alpha_{ik\sigma}^\dagger \alpha_{jp\sigma}^\dagger \alpha_{lq\sigma} \alpha_{ms\sigma} \Delta(k+p-q-s)$$
$$+ \frac{1}{N} \sum_{\substack{i,j,l,m \\ k,p,q,s}} \Gamma_{ij;lm}^\perp(kp|qs) \alpha_{ik\uparrow}^\dagger \alpha_{jp\downarrow}^\dagger \alpha_{lq\downarrow} \alpha_{ms\uparrow} \Delta(k+p-q-s), \tag{9}$$

where the initial amplitudes

$$\Gamma_{ij;lm}^\parallel(kp|qs) = V_{ij;lm}(kp|qs) = V u_{q-p} w_{i1}(k) w_{j2}(p) w_{l2}^*(q) w_{m1}^*(s), \tag{10}$$

describe the intensity of the interaction of Fermi quasiparticles with the parallel spins and the initial amplitudes

$$\Gamma_{ij;lm}^\perp(kp|qs) = V_{ij;lm}(kp|qs) + V_{ji;ml}(pk|sq) + U_{ij;lm}(kp|qs);$$
$$U_{ij;lm}(kp|qs) = U(w_{i1}(k) w_{j1}(p) w_{l1}^*(q) w_{m1}^*(s)$$
$$+ w_{i2}(k) w_{j2}(p) w_{l2}^*(q) w_{m2}^*(s)), \tag{11}$$

describe the interaction of Fermi quasiparticles with antiparallel spins. Indices i, j, l, m can take the values of 1 or 2. Note that as far as the terms $\alpha_{ik\sigma}^\dagger \alpha_{jp\sigma}^\dagger \alpha_{lq\sigma} \alpha_{ms\sigma}$ and $\alpha_{jp\sigma}^\dagger \alpha_{ik\sigma}^\dagger \alpha_{ms\sigma} \alpha_{lq\sigma}$ correspond to the same process, the effective interaction $\Gamma^\parallel$ should be written as

$$\Gamma_{ij;lm}^\parallel(kp|qs) = V_{ij;lm}(kp|qs) + (1 - \delta_{ij}\delta_{lm}) V_{ji;ml}(pk|sq). \tag{12}$$

3. Effective interaction in the Cooper channel and the equation for the order parameter

The utilization of the weak coupling Born approximation in the evaluation of the scattering amplitude in the Cooper channel allows us to limit the consideration up to the second order diagrams in the effective interaction for two electrons with the opposite values of the momentum and spin and use the quantity $\tilde{\Gamma}(p, k)$. This quantity is graphically determined as a sum of the diagrams shown in Fig. 1. Solid lines with the light (dark) arrows correspond to Green's function of the electrons with spin projections equal to $+\frac{1}{2}(-\frac{1}{2})$. It is well-known that the possibility of the Cooper pairing is determined by the characteristics of the energy spectrum close to the Fermi level and the effective interaction of
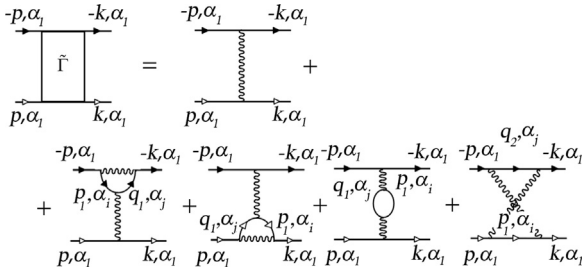
Fig. 1. First- and second-order diagrams for the effective interaction of electrons. Solid lines with the light (dark) arrows correspond to Green's functions of electrons with spin projections equal to $+\frac{1}{2}$ ($-\frac{1}{2}$) and the energy corresponding to the upper (α_1) or lower (α_2) bands in graphene. Indices i and j acquire the values 1 or 2. The momenta q_i are defined in Eq. (17).

electrons located near the Fermi surface [19]. Assuming that upon doping of graphene the chemical potential moves in the upper energy band $E_{1,k}$ and analyzing the conditions for the appearance of the Kohn–Luttinger superconductivity we may consider that the initial and final momenta will also belong to the upper band. This is shown in Fig. 1 by indices α_1 (upper band) and α_2 (lower band).

The first plot in Fig. 1 corresponds to the bare interaction of two electrons in the Cooper channel and is determined analytically by the expression

$$\tilde{\Gamma}_0(p,k) = \frac{U}{2} + \frac{V}{4}(u_{p-k}r_p^* r_k + \text{h.c.}), \tag{13}$$

where we took into account that $u_{-k} = u_k^*$. The next (Kohn–Luttinger) diagrams in Fig. 1 originate from the second-order scattering processes, $\delta\tilde{\Gamma}(p,k)$, and take into account the polarization effects of the filled Fermi sphere. In these diagrams, the presence of the two solid lines without arrows indicates the performed summation over both the values of the spin projections. Wavy lines correspond to the bare interaction. The scattering of electrons with the same spin projection gives rise only to the intersite contribution. If we have the interaction between electrons with opposite spins, the scattering amplitude is determined by the sum of the Hubbard and intersite repulsions. Therefore, when we deal only with the Hubbard repulsion, the $\delta\tilde{\Gamma}(p,k)$ correction for the effective interaction is given only by the last diagram of the exchange type. If we take into account the Coulomb repulsion at the neighboring sites, then all the diagrams in Fig. 1 contribute to the renormalized amplitude.

After the introduction of the analytical expression for the diagrams, we perform the summation over the Matsubara frequencies. Here, we take into account that the main contribution to the total scattering amplitude $\Gamma(p|k)$ in the Cooper channel comes from the scattering of electrons with the energies close to the Fermi energy, therefore, we can ignore the Matsubara frequency dependence of $\tilde{\Gamma}$ in the Bethe–Salpeter integral equation. As a result, we get the following integral expression for the effective interaction:

$$\tilde{\Gamma}(p,k) = \tilde{\Gamma}_0(p,k) + \delta\tilde{\Gamma}(p,k). \tag{14}$$

The total contribution of the second-order diagram yields

$$\delta\tilde{\Gamma}(p,k) = -\frac{1}{N}\sum_{i,j,p_1}\chi_{i,j}(q_2,p_1)\Gamma_{1i;1j}^{\perp}(p,q_2|-k,p_1)\Gamma_{j1;i1}^{\perp}(p_1,-p|q_2,k)$$

$$-\frac{1}{N}\sum_{i,j,p_1}\chi_{i,j}(q_1,p_1)\Big\{\Gamma_{1j;i1}^{\perp}(p,p_1|q_1,k)[\Gamma_{i1;j1}^{\parallel}(q_1,-p|p_1,-k)$$

$$-\Gamma_{i1;1j}^{\parallel}(q_1,-p|-k,p_1)]$$

$$+\Gamma_{i1;1j}^{\perp}(q_1,-p|-k,p_1)[\Gamma_{1j;1i}^{\perp}(p,p_1|k,q_1)$$

$$-\Gamma_{1j;i1}^{\parallel}(p,p_1|q_1,k)]\Big\}. \tag{15}$$

Here the notations for the generalized susceptibilities

$$\chi_{i,j}(k,p) = \frac{f(E_{i,k}) - f(E_{j,p})}{E_{i,k} - E_{j,p}}, \tag{16}$$

are used, where $f(x) = (\exp((x-\mu)/T) + 1)^{-1}$ is the Fermi-Dirac distribution function and the energies $E_{i,k}$ are given by formulas (6). For the sake of compactness, we introduce the following notations of the momenta combinations:

$$q_1 = p_1 + p - k; \quad q_2 = p_1 - p - k. \tag{17}$$

Knowing the renormalized expression for the effective interaction, we may proceed to the analysis of the conditions for the realization of the Cooper instability in the investigated model. It is known [19] that the appearance of the Cooper instability can be found by analyzing the homogeneous part of the Bethe–Salpeter equation. In this case, the dependence of the scattering amplitude $\Gamma(p,k)$ on momentum k is factorized and the integral equation for the superconducting gap $\Delta(p)$ is obtained. Introducing the integration over the isoenergetic contours, we reduce the investigation of the Copper instability to the solution of an eigenvalue problem [20–25]

$$\frac{1}{(2\pi)^2}\oint_{\varepsilon_{\hat{q}} = \mu}\frac{d\hat{q}}{v_F(\hat{q})}\tilde{\Gamma}(\hat{p},\hat{q})\Delta(\hat{q}) = \lambda\Delta(\hat{p}), \tag{18}$$

where the superconducting order parameter $\Delta(\hat{q})$ plays the role of the eigenvector and the eigenvalues λ satisfy the relation $\lambda^{-1} \simeq \ln(T_c/W)$. Here W is a bandwidth for both the upper and the lower branches of graphene energy spectrum determined by Eqs. (6) and (7) in case when $t_2 = 0$. In this case, the momenta $\hat{p}$ and $\hat{q}$ lie on the Fermi surface and $v_F(\hat{q})$ is the Fermi velocity.

To solve Eq. (18), we represent its kernel as a superposition of the eigenfunctions each belonging to one of the irreducible representations of the C_{6v} symmetry group on the hexagonal lattice. It is known that this group has six irreducible representations [26]: four one-dimensional and two two-dimensional. For each representation, Eq. (18) has a solution with its own effective coupling constant λ. Further on, we use the following notation to classify the symmetries of the order parameter: representation A_1 corresponds to the s-wave symmetry; B_1 and B_2, to the f-wave symmetry; E_1, to the $p+ip$-wave symmetry, and E_2, to the $d+id$-wave symmetry.

For the irreducible representation ν, we search a solution of Eq. (18) in the form

$$\Delta^{(\nu)}(\phi) = \sum_m \Delta_m^{(\nu)} g_m^{(\nu)}(\phi), \tag{19}$$

where m is the number of an eigenfunction belonging to the representation ν and ϕ is the angle defining the direction of the momentum $\hat{p}$ with respect to the p_x axis. The explicit form of the orthonormalized functions $g_m^{(\nu)}(\phi)$ is determined by the expressions

$$A_1 \to g_m^{(s)}(\phi) = \frac{1}{\sqrt{(1+\delta_{m0})\pi}}\cos 6m\phi, \quad m \in [0,\infty),$$

$$A_2 \to g_m^{(A_2)}(\phi) = \frac{1}{\sqrt{\pi}}\sin(6m+6)\phi,$$

$$B_1 \to g_m^{(f_1)}(\phi) = \frac{1}{\sqrt{\pi}}\sin(6m+3)\phi,$$

$$B_2 \to g_m^{(f_2)}(\phi) = \frac{1}{\sqrt{\pi}}\cos(6m+3)\phi,$$

$$E_1 \to g_m^{(p+ip)}(\phi) = \frac{1}{\sqrt{\pi}}(A\sin(2m+1)\phi + B\cos(2m+1)\phi),$$

$$E_2 \to g_m^{(d+id)}(\phi) = \frac{1}{\sqrt{\pi}}(A\sin(2m+2)\phi + B\cos(2m+2)\phi). \tag{20}$$

Here, for the two-dimensional representations E_1 and E_2, index m runs over the values at which the coefficients $(2m+1)$ and $(2m+2)$, respectively, are not multiple of 3.

The eigenfunctions g_m satisfy the orthonormality conditions:

$$\int_0^{2\pi} d\phi \, g_m^{(\nu)}(\phi) g_n^{(\beta)}(\phi) = \delta_{\nu\beta}\delta_{mn}. \tag{21}$$

Substituting Eq. (19) in Eq. (18), performing integration over the angles, and using condition (21), we find

$$\sum_n \Lambda_{mn}^{(\nu)}\Delta_n^{(\nu)} = \lambda_\nu\Delta_m^{(\nu)}, \tag{22}$$

where

$$\Lambda_{mn}^{(\nu)} = \frac{1}{(2\pi)^2}\oint_0^{2\pi} d\phi_{\hat{p}}\oint_0^{2\pi} d\phi_{\hat{q}}\frac{d\hat{q}}{d\phi_{\hat{q}}v_F(\hat{q})}\tilde{\Gamma}(\hat{p},\hat{q})$$
$$\times g_m^{(\nu)}(\phi_{\hat{p}})g_n^{(\nu)}(\phi_{\hat{q}}). \tag{23}$$

Since $T_c \sim W\exp(1/\lambda)$, each negative eigenvalue λ_ν corresponds to a superconducting phase with the symmetry of the order parameter of the type ν. The expansion of the order parameter $\Delta^{(\nu)}(\phi)$ in terms of the eigenfunctions generally includes many harmonics, but the main contribution is made by several terms only. The highest critical temperature corresponds to the largest absolute value of λ_ν.

4. Results and discussion

If upon doping of graphene the chemical potential moves to the upper band $E_{1,k}$, then when we analyze the conditions for the appearance of the Kohn–Luttinger superconductivity, we should consider mostly the contribution of the scattering of the electrons with the energies corresponding to the upper branch of the energy spectrum (Eq. (14) at $i=j=1$). Calculated dependences of the effective coupling constant λ on the carrier density n for the different types of symmetries of the superconducting order parameter are presented in Fig. 2. The calculation was performed for the set of parameters $t_2 = 0$, $U = 3|t_1|$, and $V = 0$. It can be seen that over the entire region of the carrier density region $1 < n < 1.25$ the superconducting phase with the f-wave symmetry of the order parameter is realized (the contribution comes from the $g_m^{(f_1)}(\phi) = (1/\sqrt{\pi})\sin(6m+3)\phi$ harmonics, whereas the contribution of the $g_m^{(f_2)}(\phi) = (1/\sqrt{\pi})\cos(6m+3)\phi$ harmonics is absent), whereas the contribution of the). Here and below, the figures show only the curves corresponding to the f-, $p+ip$-, $d+id$-symmetries which are characterized by the largest absolute values of λ_ν.
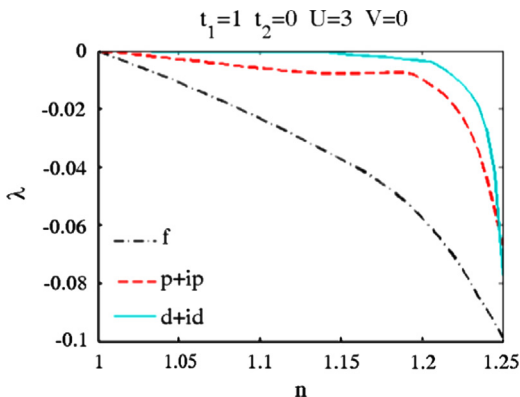
Fig. 2. (Color online) Dependences of λ on the electron density n with respect to the effective interaction of the electrons with the energies corresponding to the upper branch of the graphene energy spectrum $E_{1,k}$ for $t_2 = 0$, $U = 3|t_1|$, and $V = 0$. The leading superconducting (SC) instability for all the densities $1 < n < 1.25$ corresponds to f-wave pairing (B_1-representation of the order parameter, see Eq. (20)).
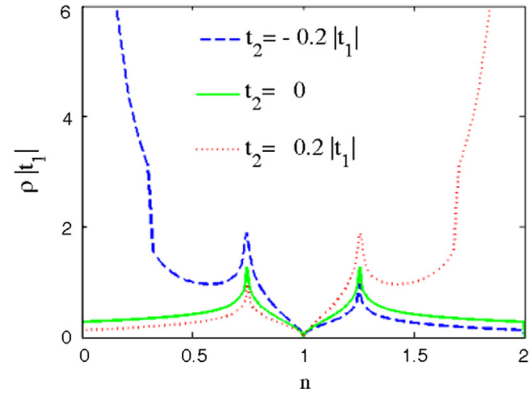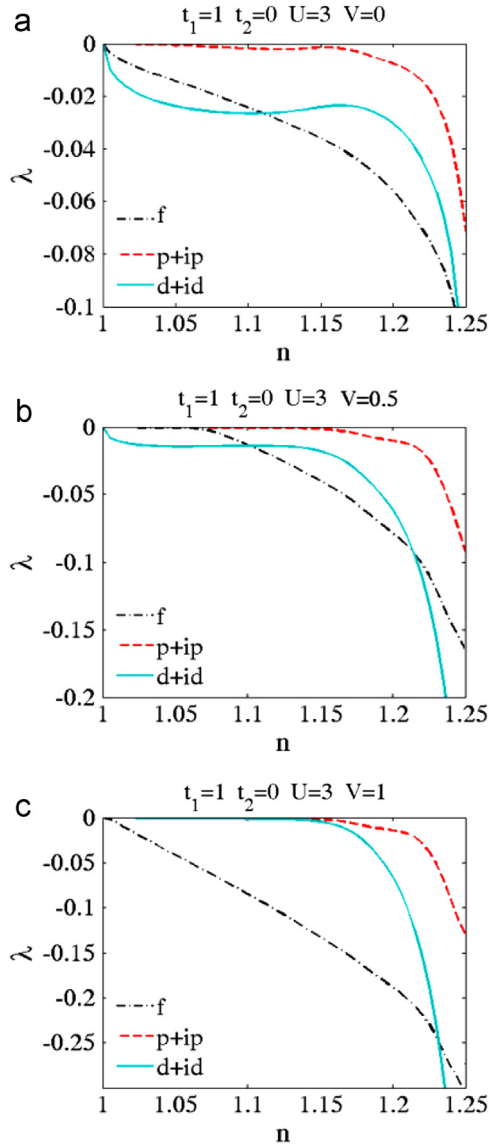

Fig. 3. (Color online) Evolution of the electron density of states of graphene with the inclusion of hoppings to the next-to-nearest-neighbor atoms.

Note that in this paper, we analyze only the range of electron densities for which we do not approach too close to the van Hove singularity (solid green curve in Fig. 3), in order to escape the summation of parquet diagrams [27,28].

The inclusion of the Coulomb interaction of electrons with the energies corresponding to different branches of the graphene energy spectrum (in this case, the effective interaction is described by the complete expression (14)) qualitatively changes the super-conducting phase diagram. In particular, at the low electron densities $1 < n < 1.13$ and near the van Hove singularity, the competition between the superconducting phase with the f-wave and $d+id$-wave symmetries occurs, which is described by the two-dimensional representation E_2 (Fig. 4). Namely for the densities $1 < n < 1.13$ the leading SC-instability corresponds to $d+id$-wave pairing, while for the densities $1.13 < n < 1.25$ we have f-wave pairing. It agrees well with the dependences $\lambda(n)$ calculated for the Hubbard model on the hexagonal lattice in paper [23].

The inclusion of the intersite Coulomb repulsion significantly affects the interplay between the superconducting phases. This is clearly seen in Fig. 4(b) and (c), where we show the dependences of $\lambda(n)$ for $V = 0.5|t_1|$ and $V = 1|t_1|$. Their comparison to the plots in Fig. 2 demonstrates that the inclusion of already weak intersite Coulomb repulsion suppresses the Cooper pairing in $d+id$-wave channel at the low densities, however it leads to realization of $d+id$-pairing near the van Hove singularity (Fig. 4 (b)). As a result, the f-wave pairing takes place for the densities $1 < n < 1.21$. A further increase in parameter V leads to the growth of the pairing intensity in both $d+id$-wave and f-wave channels at the low and intermediate electron densities (Fig. 4(c)). The leading SC-instability here corresponds to f-wave pairing for the densities $1 < n < 1.23$ and to $d+id$-wave pairing near the van Hove singu-larity. In the calculation of the dependences of $\lambda(n)$ in Fig. 4(c), we used the parameters close to those obtained from the ab initio calculation in paper [16].

The account for electron hoppings to the next-to-nearest-neighbor carbon atoms (t_2) does not qualitatively affect the inter-play of the superconducting phases (Fig. 4). This is illustrated in Fig. 5, where we show the dependences of $\lambda(n)$ for the para-meters $t_2 = 0.2|t_1|$, $U = 3|t_1|$, and $V = 0.5|t_1|$. Here again we have $d+id$-wave pairing for $1 < n < 1.12$ and $1.18 < n < 1.25$, and f-wave pairing for $1.12 < n < 1.18$. Such a behavior of the system is explained by the fact that the inclusion of the hoppings $t_2 > 0$ or $t_2 < 0$ does not significantly modify the electron density of states of graphene in the regions of the carrier concentration between the Dirac point and both points of the van Hove singularities n_{vH} (Fig. 3). However, it can be seen in Fig. 5 that the account for the hoppings t_2 leads to an increase in the absolute values of the
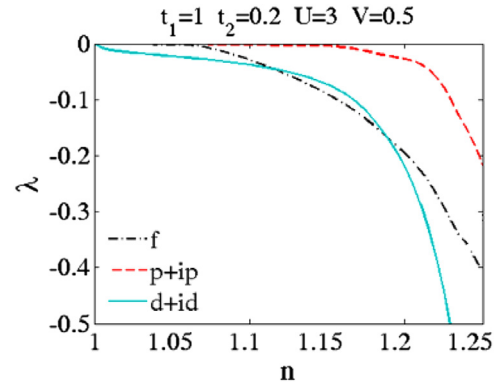
Fig. 4. (Color online) Dependences of λ on the electron density n with respect to the effective interaction of the electrons with the energies corresponding to both branches of the graphene energy spectrum for $t_2 = 0$ and $U = 3|t_1|$ at different parameters of the intersite Coulomb repulsion: (a) $V = 0$, (b) $V = 0.5|t_1|$, and (c) $V = 1|t_1|$.

Fig. 5. (Color online) Dependences of λ on the electron density n with respect to the effective interaction of electrons with the energies corresponding to both branches of the graphene energy spectrum for $t_2 = 0.2|t_1|$, $U = 3|t_1|$, and $V = 0.5|t_1|$.

symmetries of the order parameter. On the other hand, the account of the distant electron hoppings only weakly modifies the phase diagram. At the same time, it leads to an increase in the absolute values of the effective interaction and, consequently, to the higher critical temperatures (up to $T \sim 10$ K) of the superconducting transition in graphene.

It will be interesting to generalize our results on bilayer and multilayer graphene structures. Note that rigorously speaking the substantial difference between graphene and graphite manifests itself only on the level of two layers and the rotation of their elementary lattice cells with respect to each other. In bilayer and multilayer graphene, it is very important and desirable (see [29–31]) to take the interlayer Hubbard repulsion U_{12} into account and to construct the superconducting phase diagram as a function of the relative strength of the interlayer and onsite Hubbard repulsions U_{12}/U_1 and relative electron densities in the layers n_1/n_2. It will be also interesting to perform the calculations in the spirit of experiments [32] on high-T_c superconducting systems and to find a pronounced maximum in T_c as a function of the number of layers.

Acknowledgments

effective interaction and, consequently, realization of the higher critical temperatures of the transition to the superconducting phase in graphene.

5. Conclusion

Considering a monolayer of an idealized graphene and neglecting the van der Waals potential of a substrate and the role of the nonmagnetic impurities, we demonstrated that the Kohn–Luttinger superconducting pairing can be realized in the systems with the linear dispersion law. The electronic structure of graphene was described by the strong coupling Wannier representation on the hexagonal lattice within the Shubin–Vonsowsky model, which takes into account not only the intrasite, but also the intersite Coulomb repulsion. We constructed the superconductive phase diagram and demonstrated that the inclusion of the intersite Coulomb repulsion significantly changes the regions occupied by the superconducting phases with the f-, $d+id$-, and $p+ip$-wave

References

[1] Yu.E. Lozovik, S.P. Merkulova, A.A. Sokolik, Phys. Usp. 51 (2008) 727.
[2] A.H. Castro Neto, F. Guinea, N.M.R. Peres, K.S. Novoselov, A.K. Geim, Rev. Mod. Phys. 81 (2009) 109.
[3] H.B. Heersche, P. Jarillo-Herrero, J.B. Oostinga, L.M.K. Vandersypen, A.F. Morpurgo, Nature 446 (2007) 56.
[4] N.M.R. Peres, F. Guinea, A.H. Castro Neto, Phys. Rev. B 72 (2005) 174406.
[5] E.C. Marino, L.H.C.M. Nunes, Nucl. Phys. B 741 (2006) 404.
[6] J. González, F. Guinea, M.A.H. Vozmediano, Phys. Rev. B 63 (2001) 134421.
[7] B. Uchoa, A.H. Castro Neto, Phys. Rev. Lett. 98 (2007) 146801.
[8] A.M. Black-Schaffer, S. Doniach, Phys. Rev. B 75 (2007) 134512.
[9] C. Honerkamp, Phys. Rev. Lett. 100 (2008) 146404.
[10] M.L. Kiesel, C. Platt, W. Hanke, D.A. Abanin, R. Thomale, Phys. Rev. B 86 (2012) 020507(R).
[11] J. González, Phys. Rev. B 78 (2008) 205431.
[12] R.S. Markiewicz, J. Phys. Chem. Solids 58 (1997) 1179.
[13] W. Kohn, J.M. Luttinger, Phys. Rev. Lett. 15 (1965) 524.

[14] B. Valenzuela, M.A.H. Vozmediano, New J. Phys. 10 (2008) 113009.
[15] R. Nandkishore, L.S. Levitov, A.V. Chubukov, Nature Phys. 8 (2012) 158.
[16] T.O. Wehling, E. Şaşıoğlu, C. Friedrich, A.I. Lichtenstein, M.I. Katsnelson, S. Blugel, Phys. Rev. Lett. 106 (2011) 236805.
[17] S. Shubin, S. Vonsowsky, Proc. R. Soc. A 145 (1934) 159.
[18] P.R. Wallace, Phys. Rev. 71 (1947) 622.
[19] L.P. Gor'kov, T.K. Melik-Barkhudarov, Sov. Phys. J. Exp. Theor. Phys. 13 (1961) 1018.
[20] D.J. Scalapino, E. Loh Jr, J.E. Hirsch, Phys. Rev. B 34 (1986) 8190.
[21] M.A. Baranov, A.V. Chubukov, M.Yu. Kagan, Int. J. Mod. Phys. B 6 (1992) 2471.
[22] R. Hlubina, Phys. Rev. B 59 (1999) 9600.
[23] S. Raghu, S.A. Kivelson, D.J. Scalapino, Phys. Rev. B 81 (2010) 224505.
[24] M.Yu. Kagan, V.V. Val'kov, V.A. Mitskan, M.M. Korovushkin, J. Exp. Theor. Phys. Lett. 97 (2013) 226.
[25] M.Yu. Kagan, V.V. Val'kov, V.A. Mitskan, M.M. Korovushkin, J. Exp. Theor. Phys. 117 (2013) 728.
[26] L.D. Landau, E.M. Lifshitz, Quantum Mechanics: Non-Relativistic Theory, Pergamon, Oxford, 1977.
[27] I.E. Dzyaloshinskii, V.M. Yakovenko, Sov. Phys. J. Exp. Theor. 67 (1988) 844.
[28] I.E. Dzyaloshinskii, I.M. Krichever, Ya. Khronek, Sov. Phys. J. Exp. Theor. Phys. 67 (1988) 1492.
[29] M.Yu. Kagan, Phys. Lett. A 152 (1991) 303.
[30] M.Yu. Kagan, V.V. Val'kov, J. Exp. Theor. Phys. 113 (2011) 156.
[31] M.Yu. Kagan, V.V. Val'kov, Sov. Phys. Low Temp. 37 (2011) 84.
[32] I. Bozovic, J.N. Eckstein, G.F. Virshup, Physica C 235–240 (1994) 178.